Cell Reports, Volume *37*

Supplemental information

Neurovascular dynamics of repeated cortical spreading depolarizations after acute brain injury

Hanzhi T. Zhao, Mary Claire Tuohy, Daniel Chow, Mariel G. Kozberg, Sharon H. Kim, Mohammed A. Shaik, and Elizabeth M.C. Hillman

SUPPLEMENTAL FIGURES

Figure S1. Comparison of corrected GCaMP signal with and without Rose Bengal factor in a representative animal.

Figure S2. Neural activity after photothrombosis in a second representative mouse and a saline-injected control.

Figure S3. Validation of vasoconstriction calculations.

Figure S4. Summary table of all metrics used for analysis of vascular response variability to CSDs.

Figure S5. Additional examples of heterogeneous vascular responses to subsequent CSDs.

Figure S6. Characterization of the cumulative effects of successive CSDs in an awake, behaving mouse to control for effects of anesthesia.

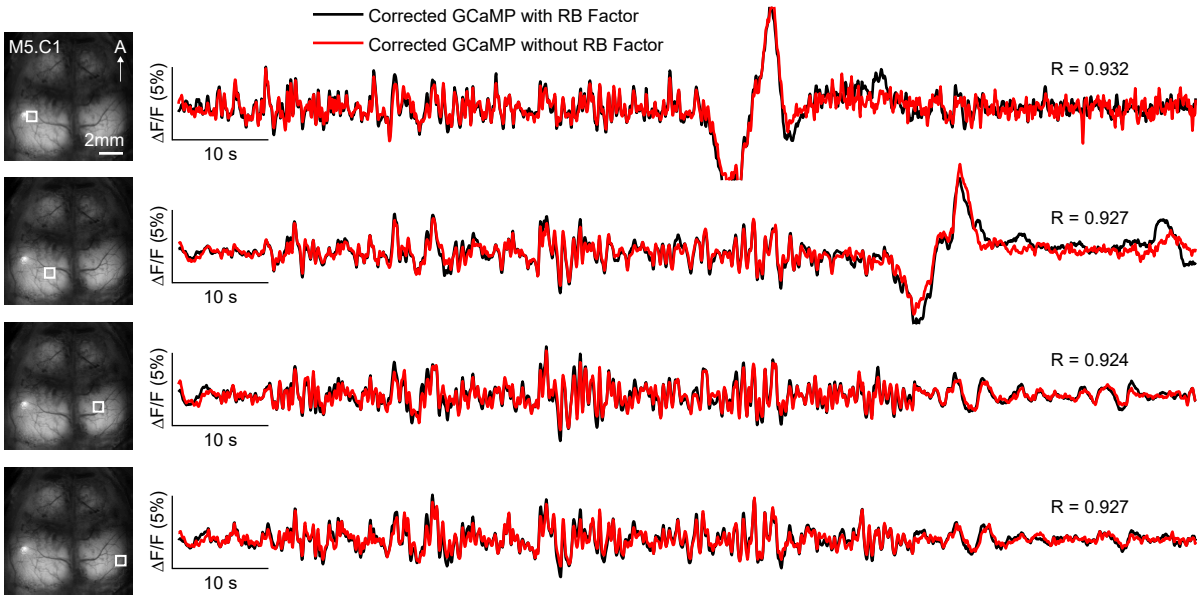

Figure S1. Comparison of corrected GCaMP signal with and without Rose Bengal factor in a representative animal. Regions both proximal and distal to the site of photothrombosis were selected as well as regions from the contralateral hemisphere. No major differences were observed in corrected GCaMP signal with or without the Rose Bengal factor across any cortical regions. Rose Bengal correction factor also did not affect any quantified measurements shown in Results, such as vessel diameters, CSD speed and residual core growth, hemodynamic response to CSDs, or post-CSD oligemia. See STAR Methods for calculations. Related to Figure 1.

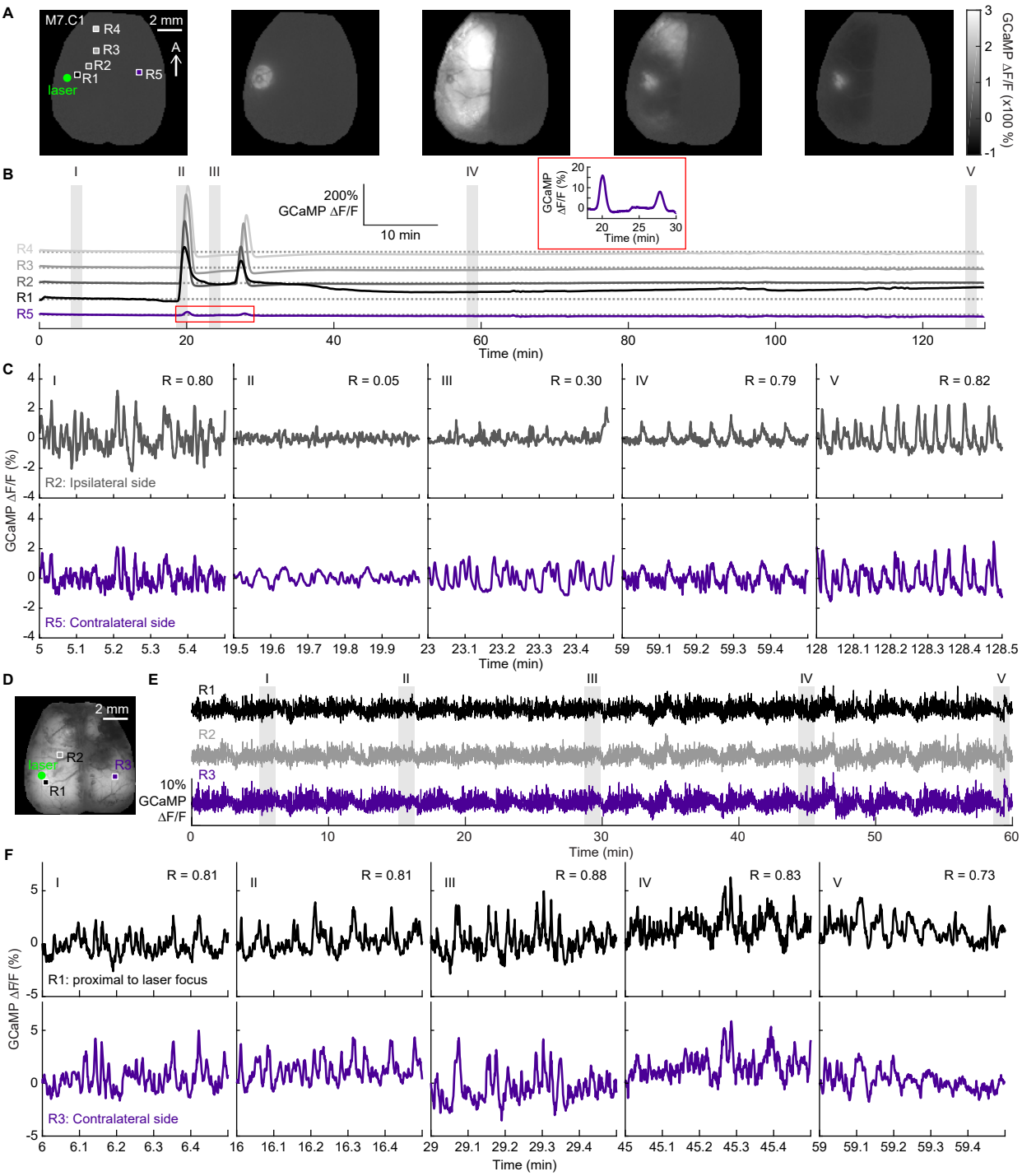

Figure S2. Neural activity after photothrombosis in a second representative mouse and a saline-injected control. (A) Spatial maps show the propagation of an initial CSD. Boxes indicate ROIs used for the traces in B. (B) Full time courses of GCaMP over 2+ hours of imaging for four ipsilateral regions and one contralateral region. Shaded areas show the specific time points highlighted in C. Note that in this mouse, and in two others (M5 and M6), a small positive GCaMP response and hyperemic HbT response were observed in the contralateral cortex (inset). The contralateral change shown was spatially diffuse and temporally delayed by 18 seconds with respect to the peak of the ipsilateral CSD. In some cases, a small representation of this delayed event was also visible in the ipsilateral GCaMP signal. (C) 30-second traces of spontaneous GCaMP activity at each time point indicated in (B) for an ipsilateral (gray) and contralateral (purple) region. (D-F) Neural activity during 532 nm laser illumination in a saline-injected control mouse. (D) Grayscale image of the exposed cortical area. Boxes show the ROIs used for the traces in E. (E) GCaMP traces for three ROIs over 60 minutes after saline-injection and turning on of the laser. Shaded areas indicate the specific time points shown in F. (F) 30-second time courses of spontaneous GCaMP activity at each of the time points indicated in (E) for one ipsilateral (black) and one contralateral (purple) region. Related to Figure 2.

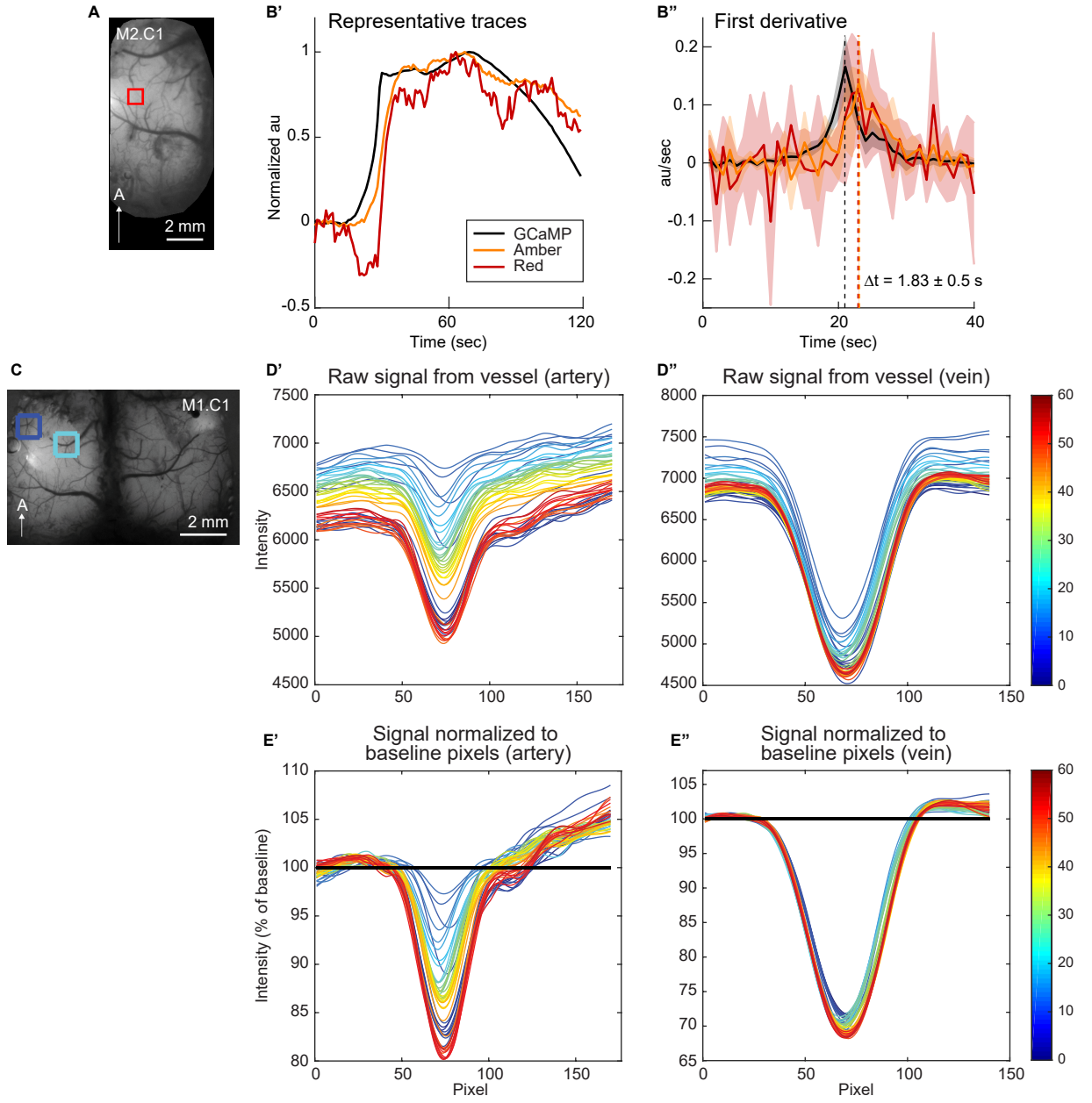

Figure S3. Validation of vasoconstriction calculations. (A) Grayscale image shows the region of interest used to compare the timings of raw fluorescence and reflectance signals. (B') Representative GCaMP fluorescence, amber, and red reflectance traces show that increases in fluorescence precede changes in hemodynamics. (B'') Onset time of the signal rise was calculated as the time at which the first derivative of the signal is maximized. The time lag between the rise of GCaMP fluorescence and amber/red reflectance averaged 1.83 sec (± 0.5 sec, n=8) across all animals. Shaded regions represent standard deviation. (C) Because there was overall brightening of the brain during a CSD, it was necessary to ensure that the observed vasoconstriction was not an optical artifact. Grayscale image of the field of view over which vessels were selected for analysis. Dark blue box highlights an example artery and cyan box highlights an example vein. Cross-sections of arteries (D') and veins (D'') were selected and each time point was plotted as a separate curve – low intensities corresponded to the vessels, while high intensities corresponded to the brighter parenchymal pixels. The color transition of the curves from blue to red represents time from 0 to 60 seconds. (E') Each curve in D was normalized to the signal from the nearby parenchymal pixels to account for global tissue intensity changes. This allowed for disambiguation of intensity changes due to constriction and global tissue brightening. The full width half max was then calculated for each curve. A reduction in the full width half max suggested a narrowing of the vessel, as shown in Figure 3A and B. (E'') Identical analysis was done for veins, where there was virtually no change in calculated diameter. Related to Figure 3 and 4.

Figure S4. Summary table of all metrics used for analysis of vascular response variability to CSDs. Bar plots show onset speed (teal), duration (grey), and amplitude (pink) for every CSD in every mouse. See STAR Methods for details on how the plotted metrics were calculated. Icons indicate the type of hemodynamic response that occurred for a given event. X's indicate ROIs that were excluded from the averages in Figure 5B and C. Solid X's represent regions where persistent depolarization resulted in a lack of increased fluorescence during the CSD; Dashed X's represent regions that were not impacted by a given CSD. Time stamps (t = # min) indicate when each CSD occurred relative to when the photothrombosis laser was turned on. The grayscale map shows the locations for each ROI relative to the laser induction site in a representative mouse. Related to Figure 5 and 6.

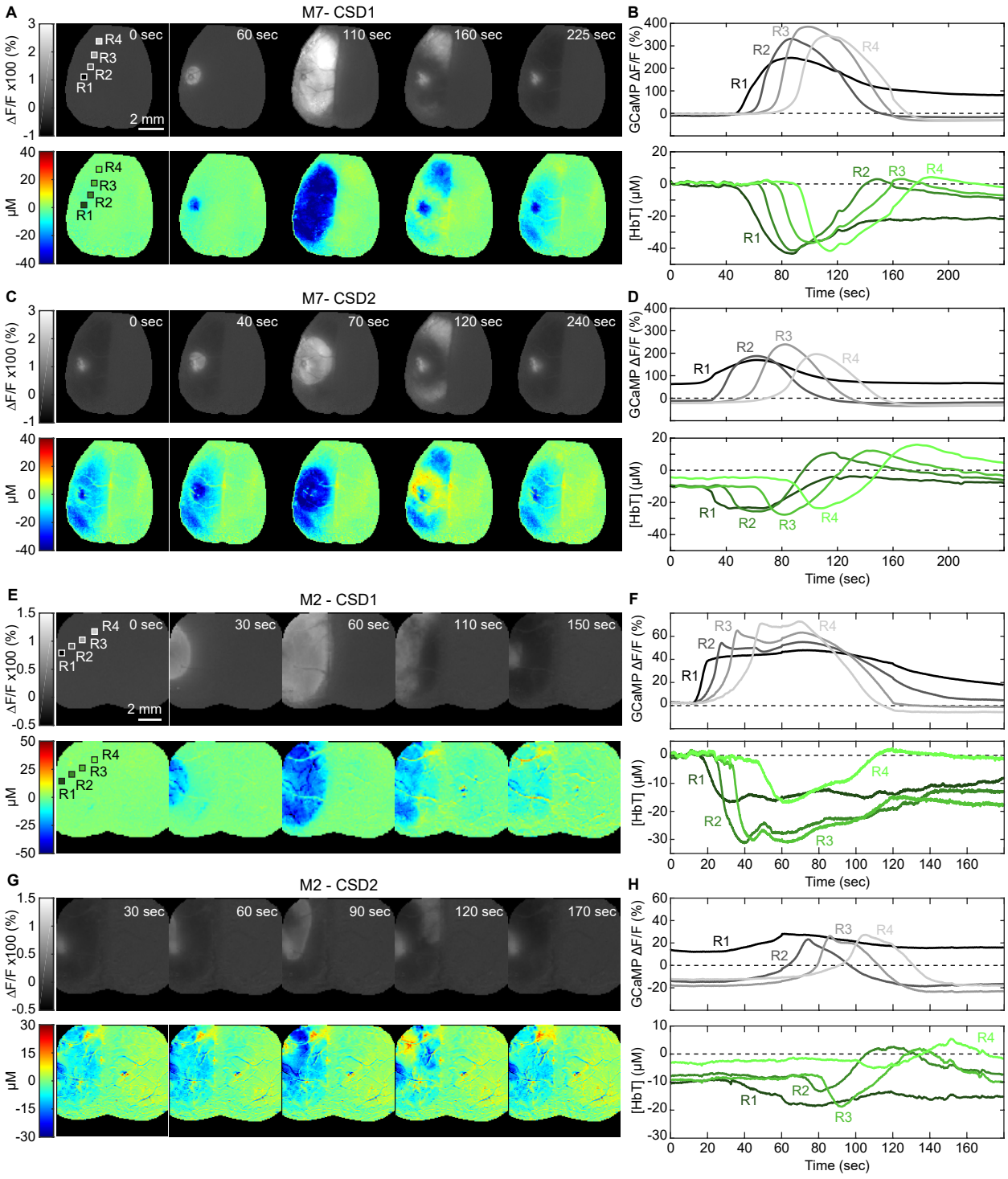

Figure S5. Additional examples of heterogeneous vascular responses to subsequent CSDs. (A) Cortical maps and (B) time courses show GCaMP (top) and [HbT] (bottom) during the initial CSD of an example mouse. (C) Cortical maps and (D) time courses of GCaMP and [HbT] during the second CSD in the same mouse. (E-H) Cortical maps and time courses for both the initial CSD and a second CSD in another example mouse. GCaMP maps in both additional examples reaffirm that initial CSDs spread uniformly and radially. Total hemoglobin maps and time courses confirm that hemodynamic responses to initial CSDs are vasoconstrictive. In these examples, the second CSDs showed varying propagation patterns with M7 beginning radially and eventually forming a ring, and M2 spreading mostly into anterior territories and leaving posterior ones unaffected. Hemoglobin maps and traces show that different regions within the same event can exhibit different hemodynamic responses. Plot of total hemoglobin for M2 - CSD2 (H, bottom) shows one vasoconstrictive region and three biphasic regions. Related to Figure 5, see also STAR Methods.

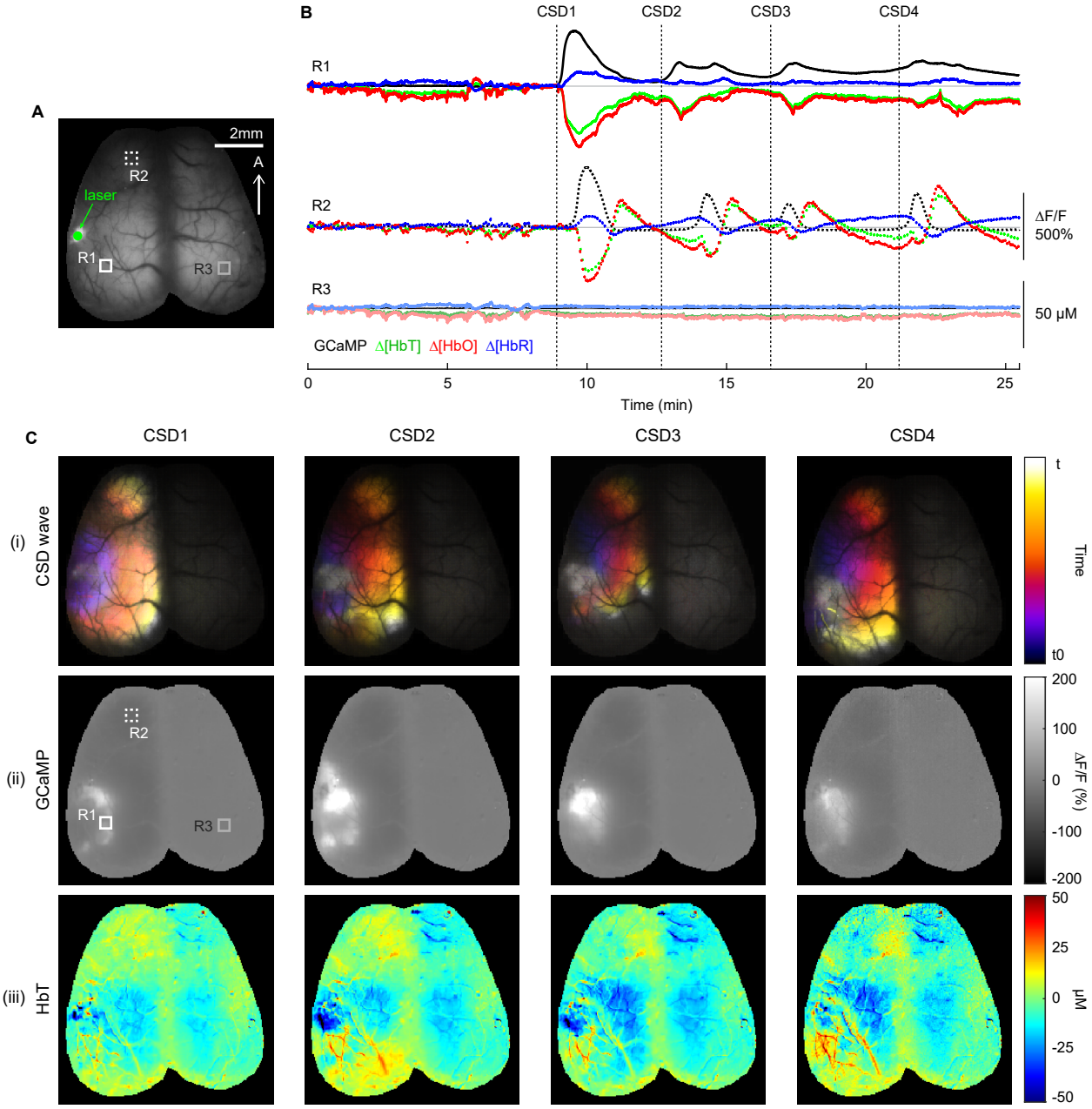

Figure S6. Characterization of the cumulative effects of successive CSDs in an awake, behaving mouse to control for effects of anesthesia. (A) Grayscale cortical map shows imaging field of view and the ROIs used for the time courses in B relative to the laser focus, indicated by the green dot. (B) GCaMP ΔF/F, [HbT], [HbO], and [HbR] traces extracted from the regions indicated in A. Saturated time courses were extracted from two ipsilateral regions and faded time courses were extracted from the contralateral region. (C) (i) Cortical maps color-coded by time, showing the propagation dynamics of each CSD for this mouse, which had four total CSDs. (ii-iii) Cortical maps showing post-CSD levels of GCaMP ΔF/F (ii) and [HbT] (iii) 5 seconds after the completion of each CSD event. The spatial maps highlight the growing areas of elevated GCaMP fluorescence and accompanying oligemia after each successive CSD. These results recapitulate those described in Figure 6, suggesting that the cumulative impacts observed were not due to urethane anesthesia. Related to Figure 6.